ADVANCED BIOLOGY
www.advanced-bio.com

A Microfluidics-Based Screening Tool to Assess the Impact of Blood Plasma Factors on Microvascular Integrity

*Abidemi Junaid, Vincent van Duinen, Wendy Stam, Sophie Dólleman, Wei Yang, Yolanda de Rijke, Hendrik Endeman, Cees van Kooten, Alireza Mashaghi, Hetty de Boer, Janine van Gils, Thomas Hankemeier, and Anton Jan van Zonneveld**

This study provides a method to assess the impact of circulating plasma factors on microvascular integrity by using a recently developed microvessel-on-a-chip platform featuring the human endothelium that is partly surrounded by the extracellular matrix. The system is high-throughput, which allows parallel analysis of organ-level microvessel pathophysiology, including vascular leakage. Ethylenediaminetetraacetic acid plasma samples are mixed with inhibitors for recalcification of the plasma samples to avoid activation of the coagulation- or complement system. Moreover, the assay is validated by spiking vascular endothelial growth factor, histamine, or tumor necrosis factor alpha to recalcified plasma and confirms their modulation of microvessel barrier function at physiologically relevant concentrations. Finally, this study shows that perfusing the microvessels with recalcified plasma samples of coronavirus disease-2019 patients, with a confirmed proinflammatory profile, results in markedly increased leakage of the microvessels. The assay provides opportunities for diagnostic screening of inflammatory or endothelial disrupting plasma factors associated with endothelial dysfunction.

1. Introduction

Cardiovascular diseases cause health and economic burdens worldwide.[1] In patients, impaired microvascular integrity is often associated with elevated plasma levels of proinflammatory compounds, such as vascular endothelial growth factor (VEGF), tumor necrosis factor alpha (TNFα), and Interleukin 6 (IL-6). These factors can drive microvascular leakage, angiogenesis or inflammation.[2–4] In our previous work, we developed 3D microvessels-on-chips to study the responses of the vasculature to pro-inflammatory factors such as TNFα.[5] Moreover, we demonstrated that the microvessel-on-a-chip technology can be used as an experimental human model for Ebola haemorrhagic fever, showing vascular leakage.[6] However, disease-related circulating factors that adversely impact vascular integrity due to imbalance in concentrations are often highly complex. Therefore, instead of measuring the impact of individual cytokines or growth factors on vascular homeostasis, the availability of ethylenediaminetetraacetic acid (EDTA) plasma provides the opportunity to assess the overall effect of all circulating vasoactive and inflammatory factors on the microvascular function. EDTA is a scavenger of metal ions and

A. Junaid, W. Yang, A. Mashaghi, T. Hankemeier
Division of Systems Biomedicine and Pharmacology
Leiden Academic Centre for Drug Research
Leiden University
Leiden 2333 CC, The Netherlands

A. Junaid, V. van Duinen, W. Stam, S. Dólleman, C. van Kooten, H. de Boer, J. van Gils, A. J. van Zonneveld
Department of Internal Medicine (Nephrology)
Leiden University Medical Center
Leiden 2333 ZA, The Netherlands
E-mail: a.j.vanzonneveld@lumc.nl

The ORCID identification number(s) for the author(s) of this article can be found under https://doi.org/10.1002/adbi.202100954.

DOI: 10.1002/adbi.202100954

A. Junaid, V. van Duinen, W. Stam, S. Dólleman, C. van Kooten, H. de Boer, J. van Gils, A. J. van Zonneveld
Einthoven Laboratory for Vascular and Regenerative Medicine
Leiden University Medical Center
Leiden 2333 ZA, The Netherlands

Y. de Rijke
Department of Clinical Chemistry
Erasmus MC
University Medical Center Rotterdam
Rotterdam 3015 GD, The Netherlands

H. Endeman
Department of Intensive Care
Erasmus MC
University Medical Center Rotterdam
Rotterdam 3015 GD, The Netherlands

suppresses intercellular contacts.[7,8] We circumvent the activation of the coagulation and complement systems by developing a protocol to recalcify EDTA plasma that is compatible with microvessel culture. Here, we demonstrate that using specific inhibitors, microvessels exposed to recalcified plasma retain their integrity and allow for the assessment of the impact of disease-related plasma constituents in the microvessels-on-chips. We validated our method by perfusing plasma samples of patients infected with severe acute respiratory syndrome coronavirus 2 (SARS-CoV-2) in the microvessels. These diseased microvessels, as a result of the addition of patient plasma, showed increase in permeability and resembled vascular dysfunction as seen in vivo.

2. Results

2.1. Design of a Functional Microvessel-on-a-Chip

To generate human microvessels-on-chips, we used the fabricated OrganoPlates (T-design) of MIMETAS that are based on a 384-well microtiter plate format and employs coverslip-thickness glass (175 µm) for optical access.[9] A plate comprises microfluidic tissue chips, that can be used to establish 96 microvessels with heights of 120 µm and widths of 400 µm (**Figure 1**A). Each chip contains a phaseguide for adjusting the capillary pressure to pattern type 1 collagen in the extracellular matrix (ECM) channel (Figure 1B; Figure S1, Supporting Information). The

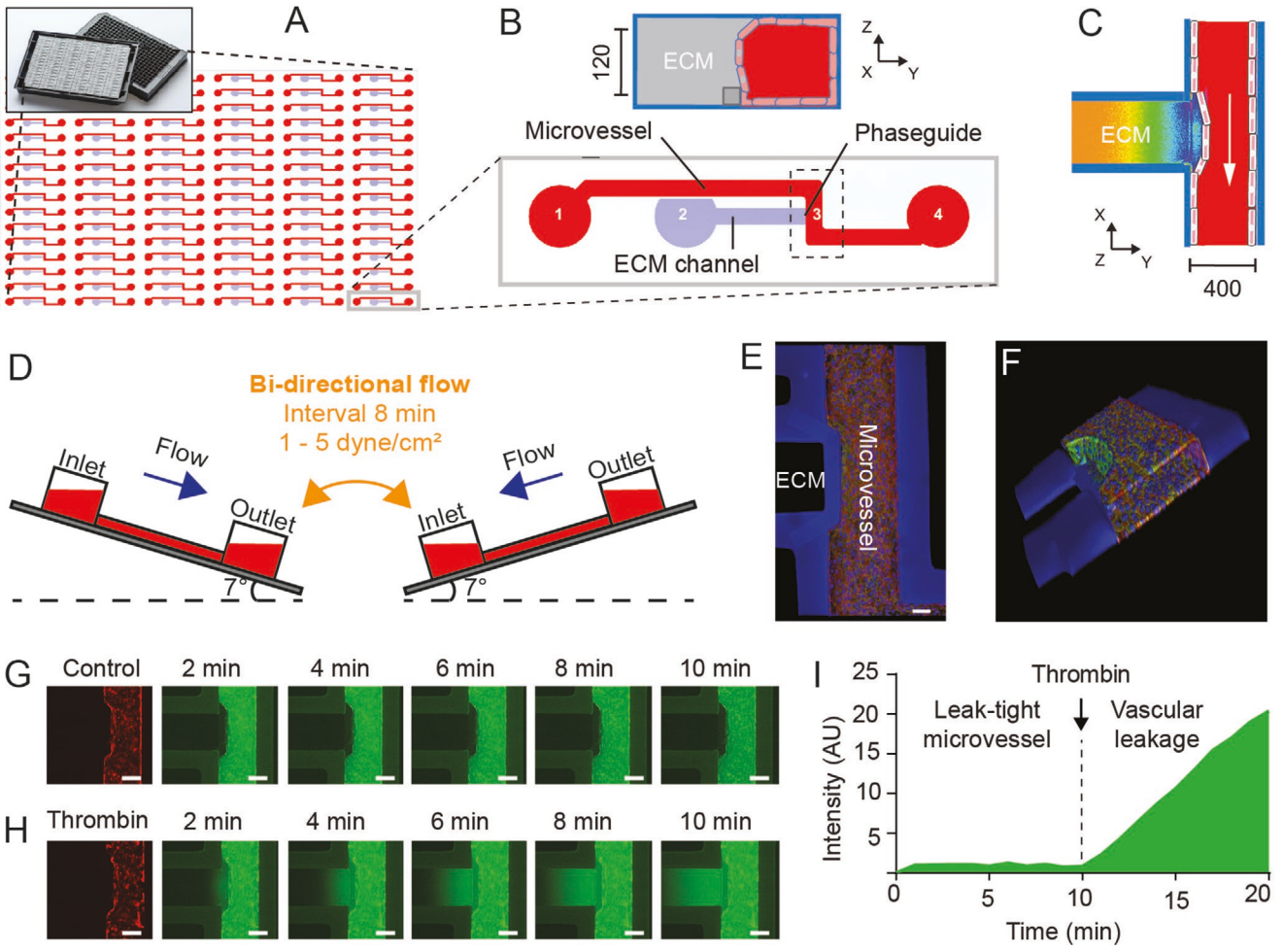

Figure 1. The human microvessel-on-a-chip. A) Schematic diagram of 96 microfluidic tissue chips that compromise a gradient design (T-design) in the OrganoPlate. The highlighted rectangular box shows the area depicted in (B). B) Diagram of a single chip; 1 = medium inlet, 2 = gel inlet, 3 = observation window, 4 = medium outlet. The inlay shows the compartments of the microvessel and the ECM. The dashed rectangular box highlights the region shown in (C) and (E). C) Fluorescent intensity profile illustrating the distribution of albumin in a 3D collagen ECM region under experimental conditions. Bluish colors indicate higher fluorescent intensities. D) Fluid shear stress in the OrganoPlate is induced by a bidirectional flow generated by leveling with the rocker platform. E) Cultured HUVECs formed (red, F-actin) a microvessel that exhibited continuous intercellular junctions on-chip, as demonstrated by VE-cadherin staining (green). Scale bar: 100 µm. F) A 3D reconstruction showing the human microvessel-on-a-chip. G) Time-lapse fluorescent images of albumin (green) diffusing from the microvessel (red, left image) to the ECM channel. Scale bar: 200 µm. H) Time-lapse fluorescent images of albumin (green) diffusing from the microvessel (red, left image) to the ECM channel after treatment with 10×10^{-9} M thrombin for 20 min. Scale bar: 200 µm. I) Fluorescent intensity profile of 16 measurements in (G) and (H), illustrating leak-tight microvessels and vascular leakage after treatment with 10×10^{-9} M thrombin. There was a sharp increase in albumin concentration across the endothelial monolayer and a steady diffusive flux inside the 3D ECM.

ECM channel enables diffusion-based solute flux across the endothelial monolayer that was used to measure the endothelial permeability (Figure 1C). After seeding the collagen, we cultured primary human umbilical vein endothelial cells (HUVECs) in the perfusion channel. For easier operation of the chips, the OrganoPlate was placed on a rocker platform to create height differences between the wells which results in a gravity driven, continuous and bidirectional flow (Figure 1D). After five days in culture, immunofluorescence confocal microscopic analysis showed cortical staining of F-actin and VE-cadherin that confirmed a quiescent endothelial phenotype with intact adherens junctions (Figure 1E,F). The quiescent endothelial phenotype formed a robust endothelial barrier or leak-tight microvessel that restricted the passage of fluorescent albumin (67 kDa) between the endothelial monolayer and the ECM channel for 10 min (Figure 1G,I; Video S1, Supporting Information). The endothelial barriers were disturbed with 10×10^{-9} M thrombin for 20 min, with a subsequent increase in endothelial permeability and vascular leakage (Figure 1H,I; Video S2, Supporting Information).

2.2. Measurement of Endothelial Cell Activation in the Microvessel-on-a-Chip

Besides thrombin, more compounds in human plasma that have a known influence on endothelial permeability were assessed, including VEGF, histamine, and TNFα. VEGF promotes leakage of plasma components by perturbing endothelial barrier integrity. This protein activates endothelial cells by inducing phosphorylation and internalization of VE-cadherin.[10,11] In vivo, histamine is known as inflammatory response factor. It is a mediator of allergic inflammation that increases vascular permeability by changing VE-cadherin localization at endothelial cell junction.[12] Endothelial cell activation often involves the exposure of NADPH oxidase (NOX) to cytokines, such as TNFα, which then induces oxidative stress and at the end vascular leakage of plasma fractions.[13,14]

As shown in **Figure 2**A, human microvessels-on-chips perfused with VEGF, histamine or TNFα displayed marked increase in vessel permeability with a dose dependency in line with transendothelial electrical resistance (TEER) measurements (Figure 2B; Figure S2, Supporting Information). Immunofluorescence staining demonstrated that VEGF, histamine or TNFα-induced leakage were associated with the formation of F-actin stress fibers and redistribution of VE-cadherin into a zig-zag pattern with visible gaps between the cells, indicating internalization of VE-cadherin (Figure 2C). These results are consistent with the findings from past studies that VEGF, histamine, and TNFα induce vascular leakage in vivo at similar dosing.[12,15,16] Therefore, our findings validate that the human microvessel-on-a-chip can potentially be used to study functional aspects of human microvessels.

2.3. Development of a Method to Perfuse EDTA Plasma in the Microvessel-on-a-Chip

Being able to perfuse the microvessels and measure vascular leakage, our next goal was to introduce human blood plasma in the model. Since the EDTA present in clinical plasma samples rapidly leads to disruption of endothelial cell–cell and cell–matrix contacts by the scavenging of calcium ions (**Figure 3**AB), recalcification is a prerequisite for perfusion of EDTA plasma samples through the microvessel. However, recalcification of EDTA plasma immediately activates the procoagulant cascades thereby generating Xa and thrombin that, through the activation of the endothelial protease activated receptors (PARs), disrupt the integrity of the endothelial barrier function (Figure 3C).

To protect the integrity of the endothelial microvessels from these procoagulant factors, we used a combination of the anticoagulants hirudin and corn trypsin inhibitor (CTI). Hirudin specifically binds to, and inhibits the activity of thrombin with high affinity. We demonstrated that from a concentration of 1×10^{-6} M, hirudin extends the 50% plasma clotting time effectively (Figure 3E). Also, the intrinsic coagulation pathway is potentially activated in our microfluidic system, because of the negative charged glass surface. CTI is a specific human factor XIIa inhibitor and when added to plasma, it prolonged the activated partial thromboplastin time (aPTT) in a dose dependent fashion (Figure 3F). Besides coagulation, when combining plasma with allogenic primary endothelial cells, complement activation can take place. To prevent complement activation, we used compstatin, a C3-targeting complement inhibitor.[17,18] We observed that compstatin at concentrations of 5×10^{-6} M and higher could completely inhibit C3 deposition from recalcified EDTA plasma in an enzyme-linked immunosorbent assay (ELISA)-based classical pathway activity assay (Figure 3G).

Next, we showed that by adding 1×10^{-6} M hirudin, 50 μg mL CTI and 25×10^{-6} M compstatin, recalcified EDTA plasma could be applied to the endothelial monolayers for 18 h with full maintenance of its quiescent phenotype as evidenced by the presence of undisturbed VE-cadherin adherens junctions and cortical actin staining (Figure 3D). Also, perfusing the microvessels with recalcified inhibitor-containing EDTA plasma of healthy donors maintained leak-tight vessels (Figure S3, Supporting Information). Hence, we concluded that adding these inhibitors to recalcified EDTA plasma facilitates the assessment of the impact of circulating disease-related factors on microvessel-on-a-chip integrity.

As a proof of concept, we spiked the recalcified inhibitor-containing plasma samples of healthy donors with increasing doses of VEGF, histamine and TNFα and perfused these samples through the microvessels. As shown in **Figure 4**A, the spiked microvessels lost their leak-tightness in a dose-dependent fashion. This was especially significant for microvessels with TNFα. The permeability was not significant in samples spiked with VEGF or histamine. There might be factors in plasma samples that inhibit the effect of histamine and VEGF on vessel permeability. As a confirmation we also validated the experiment with the TEER system. Again, VEGF, histamine, and TNFα spiked in EDTA plasma effectively decreased the endothelial barrier function (Figure 4B; Figure S4, Supporting Information) corroborating the increased vessel permeability seen in the microvessels-on-chips. Importantly, the increased barrier permeability was associated with the formation of stress fibers and rearrangement of VE-cadherin (Figure 4C).

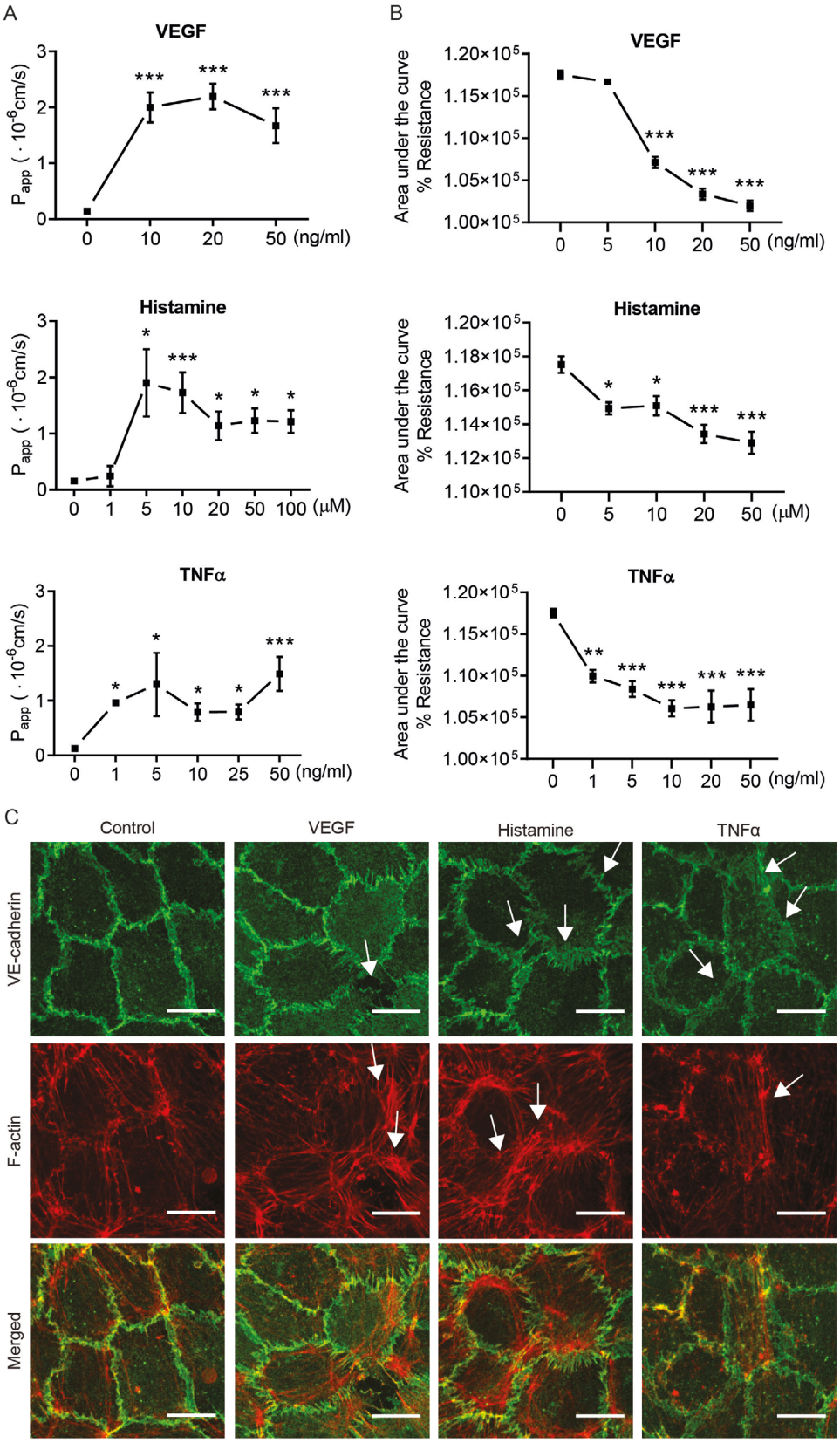

Figure 2. Modeling microvascular dysfunction in microvessel-on-a-chip. A) Dose response to VEGF, histamine, and TNFα in microvessels. Microvessels were treated for 1.5 h with VEGF, 1 h with histamine or overnight with TNFα at 37 °C, followed by vascular leakage assay. Data are presented

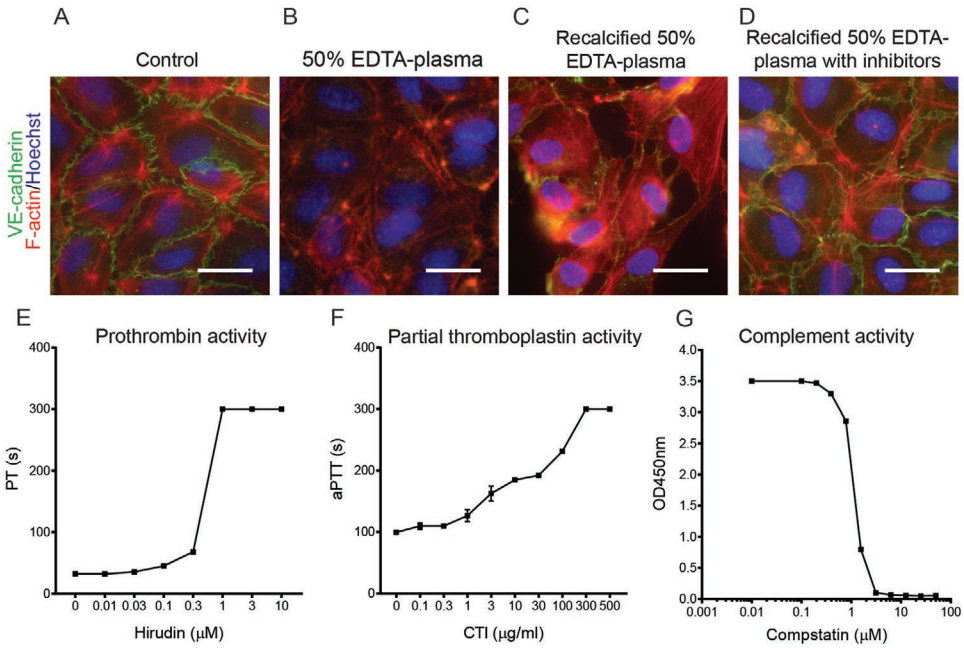

Figure 3. Coagulation and complement inhibitors for use in EDTA-plasma in vitro biocompatibility models. A–D) Immunostaining of HUVECs in the microvessels-on-chips exposed to endothelial cell culture media (control), 50% EDTA-plasma, recalcified 50% EDTA-plasma, and recalcified 50% EDTA-plasma with 1×10^{-6} M hirudin, 50 μg mL^{-1} CTI and 25×10^{-6} M compstatin. Images are representative of experiments performed on cells from three different donors. Scale bars: 50 μm. E) Effect of hirudin on prothrombin time (PT) of recalcified EDTA plasma cocktail, measured with the STart Max (Diagnostica Stago). F) Effect of CTI on the activated partial thromboplastin time (aPTT) of recalcified EDTA-plasma cocktail, measured with the STart Max (Diagnostica Stago). G) Dose-dependent inhibition of classical pathway complement activity by compstatin, as quantified by the deposition of C3. Data are presented as mean ± SEM; $n = 2$.

2.4. Recapitulation of the Effects of COVID-19 Plasma on Vascular Function

Having established the conditions to use the human microvessel-on-a-chip to study the impact of circulating disease factors on vessel permeability of 96 microvessels in parallel, we next assessed whether we would be able to also detect microvascular destabilization when perfusing plasma samples of patients with coronavirus disease-2019 (COVID-19).

Infection with SARS-CoV-2 is a life-threatening systemic disease that, in its later stages, causes severe vascular leakage in the lungs, contributing to acute respiratory distress syndrome (ARDS).[19] Utilizing a 2-lane OrganoPlate format to study vascular permeability (Figure S5, Supporting Information),[20] we perfused recalcified control plasma, and pooled plasma from COVID-19 patients with early stage disease ($n = 8$), having a marked thrombotic disorder,[21] and patients who are in a pro-inflammatory state (cytokine storm; $n = 8$). To exclude variations introduced by different HUVEC donors, pooled HUVECs (3–6 donors) were used to generate the microvessels. After 4 h of exposure to plasma from healthy controls and, early stage (ES) and late stage (LS) COVID-19, the microvessels with COVID-19 plasma samples, but not healthy controls, showed significant increase in vessel permeability. In addition, compared to the ES COVID-19, microvessels of the LS COVID-19 experienced more severe barrier disruption (**Figure 5**A). Immunohistochemical staining confirmed the disruption of the endothelial barrier in the COVID-19 plasma exposed microvessel with dissociation of the VE-cadherin adherens junctions and the formation of stress fibers (Figure 5B).

In our previous work, we established a method to measure inflammation associated bioactive lipids in microvessels cultured in the 2-lane OrganoPlate of MIMETAS by using an optimized ultraperformance liquid chromatography-tandem mass spectrometer (UPLC-MS/MS).[5] To further show the impact of COVID-19 patient plasma on the microvessel properties, we measured the secretion of Prostaglandin F2α (PGF2α), an oxidative stress marker[5,22] and showed that exposure of the microvessels to late stage COVID-19 plasma, but not to the early stage samples, led to an increase in PGF2α secretion confirming a proinflammatory phenotype of the microvessel (Figure 5C).

as mean ± SEM; $n = 6$–19 (independent chips using HUVECs from 3 to 6 different donors). Significance determined by ANOVA and Dunnett's test; $^*P < 0.05$, $^{***}P < 0.001$. B) The effects of VEGF, histamine, and TNFα on endothelial barrier function were measured in the electric cell-substrate impedance sensing (ECIS) at different doses. Area under the curve analysis after the addition of treatment. Data are represented as mean ± SEM and representative of 3–4 independent experiments performed on cells from three different donors. Significance determined by ANOVA and Dunnett's test; $^*P < 0.05$, $^{**}P < 0.01$, $^{***}P < 0.001$. C) Morphology of endothelial cells in the microvessels-on-chips in response to 10 ng mL^{-1} VEGF (1.5 h), 10×10^{-6} M histamine (1 h), and 10 ng mL^{-1} TNFα (overnight) showing VE-cadherin (green) and F-actin (red). These permeability factors induced morphological rearrangement of VE-cadherin and F-actin (arrow). Scale bars: 50 μm.

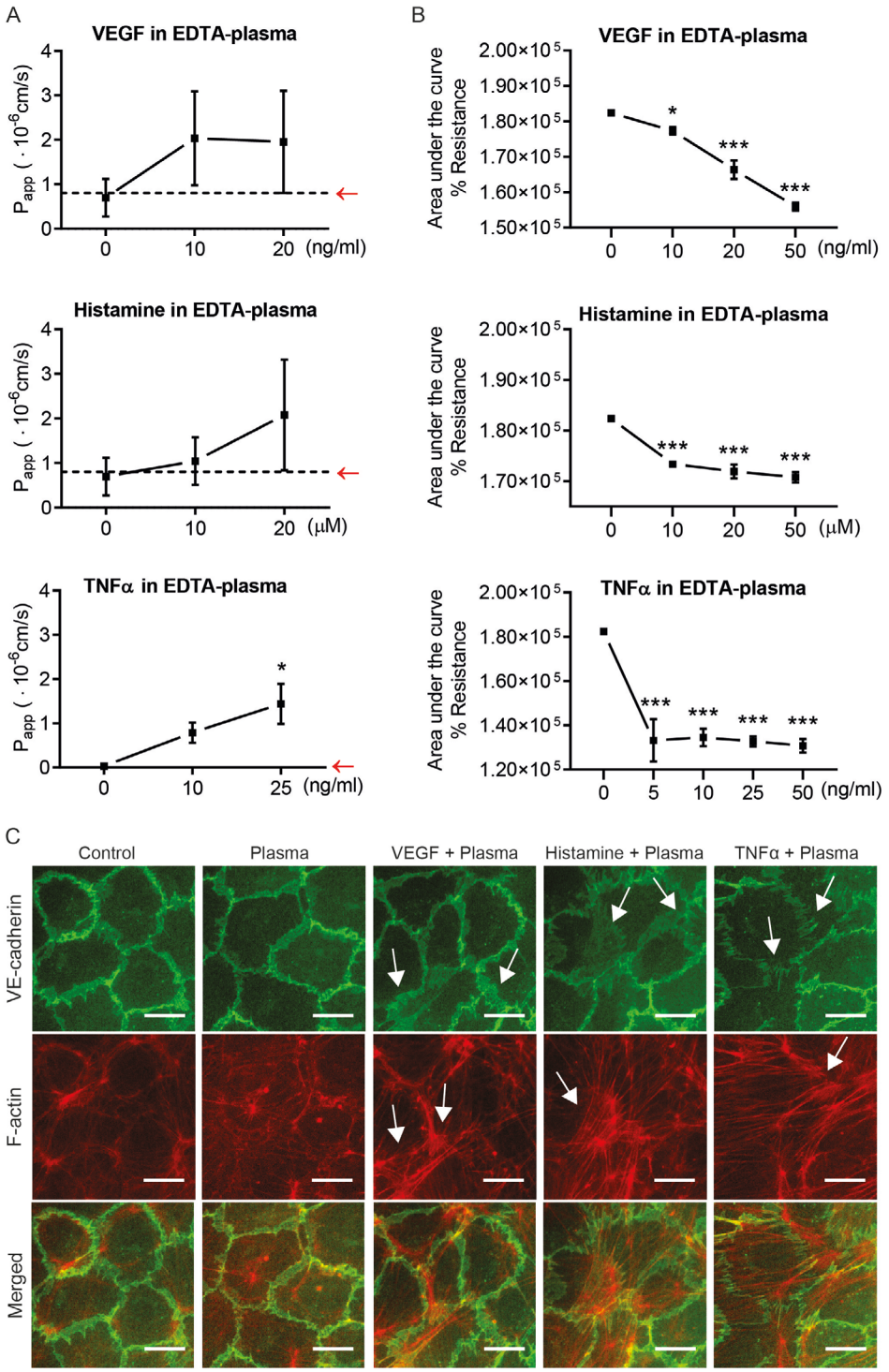

Figure 4. Permeability effect of perfusing blood plasma in microvessel-on-a-chip. A) Dose response to VEGF (1.5 h), histamine (1 h), and TNFα (overnight) spiked at several concentrations in EDTA plasma treated with 1×10^{-6} M hirudin, 50 μg mL^{-1} CTI, and 25×10^{-6} M compstatin. Red arrows indicate permeability of microvessels perfused with EGM2. Data are presented as mean ± SEM; $n = 6$ (independent chips using HUVECs from two different donors). Significance determined by ANOVA and Dunnett's test; *$P < 0.05$. B) The effects of VEGF, histamine, and TNFα spiked in EDTA plasma on endothelial barrier function were measured in the electric cell-substrate impedance sensing (ECIS) at different doses. Area under the curve analysis after the addition of treatment. Data are represented as mean ± SEM of 3–4 technical replicates and representative of 3–4 independent experiments performed on cells from three different donors. Significance determined by ANOVA and Dunnett's test; *$P < 0.05$, ***$P < 0.001$. C) Immunostaining of endothelial cells in the microvessels-on-chips for VE-cadherin (green) and F-actin (red) after treatment with 10 ng mL^{-1} VEGF (1.5 h), 10×10^{-6} M histamine (1 h) and 10 ng mL^{-1} TNFα (overnight) spiked in EDTA plasma treated with hirudin, CTI, and compstatin. VEGF, histamine, and TNFα lead to increase in actin stress fiber formation (arrowheads) and morphological rearrangement of VE-cadherin were observed. Scale bars: 50 μm.

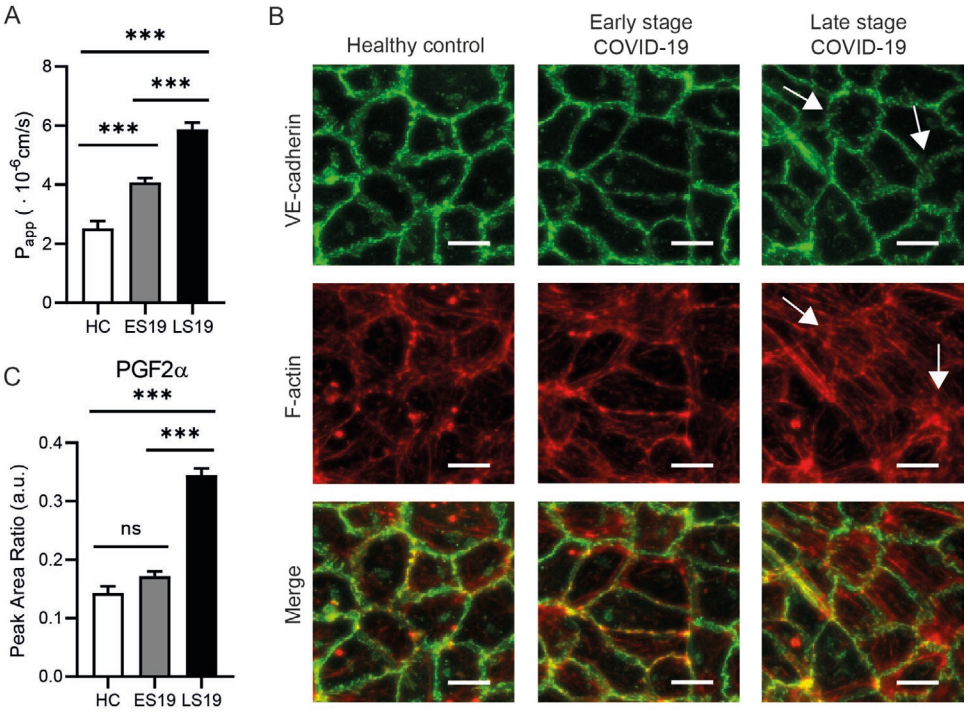

Figure 5. Impact of COVID-19 plasma samples on microvessel-on-a-chip. A) Vessel permeability after 4 h incubation of microvessels with healthy control (HC), early (ES19, 8 patients), and late (LS19, 8 patients) stages COVID-19 pooled plasma samples. Data are presented as mean ± SEM of seven independent chips. Significance determined by ANOVA and Tukey's multiple comparison test; ***$P < 0.001$. B) Immunostaining of endothelial cells in the microvessels-on-chips for VE-cadherin (green) and F-actin (red) after incubation with healthy control, early and late stages COVID-19 plasma samples. In microvessels treated with COVID-19 plasma samples an increase in actin stress fiber formation (arrowheads) and morphological rearrangement of VE-cadherin were observed. Scale bars: 50 µm. C) Peak area ratio of PGF2α secreted by the microvessels after 4 h incubation of microvessels with healthy control (HC), early (ES19, 8 patients) and late (LS19, 8 patients) stages COVID-19 pooled plasma samples. Data are presented as mean ± SEM of four pooled chips of three independent experiments. Significance determined by ANOVA and Tukey's multiple comparison test; ns = not significant, ***$P < 0.001$.

3. Discussion

Despite progress in identifying critical regulators of endothelial permeability, less is known about how in various disease states, these factors act together on the integrity of the endothelial barrier. Here, we introduced a novel approach using a microfluidic-based in vitro assay, microvessel-on-a-chip, that enabled parallel culture, real-time visualization and simultaneous quantification of endothelial permeability. Since the area of cells in contact with the ECM is small, the OrganoPlate T-design enabled us to easily create leak-tight microvessels. This design provides a more robust quantification of vessel permeability that is comparable to the OrganoPlate 2-lane.[20] We showed that VEGF, histamine, and TNFα modulate the endothelial barrier in our models at about similar concentrations as shown in in vivo studies.[23–25] This supports the potential physiological relevance of our platform technology to study key mechanisms behind the onset and progression of microvascular diseases.

Previous studies of endothelial permeability with microfluidic-based approaches were largely done by perfusing cell culture media in the system.[26–28] However, we developed a novel method to directly screen vascular diseases by using primary endothelial cells and blood. In this procedure, we extracted plasma from blood in EDTA-tubes, applied the relevant additions and perfused it in the cultured human microvessels. To prevent blood plasma from clotting, we primarily inhibited thrombin with the high-affinity inhibitor hirudin. Next to that, given the negative charged surface of the microchannels of the OrganoPlate, we inhibited the intrinsic pathway of coagulation with CTI. To prevent complement activation when combining plasma with allogenic primary endothelial cells, we used compstatin to inhibit the complement cascade at the most central component, being C3.[29]

There are protocols available for perfusing whole blood in in vitro vessel systems.[30,31] However, these protocols differ, ignoring contact and complement activation. This limits the perfusion of whole blood in the system for a very short time (≈20 min) before experiencing clotting. With our protocol, we can perfuse plasma in the chip for 24 h for long-term studies. Methods to recalcify plasma samples for subsequent assessment on endothelial cell-based assay have been performed but not with the same approach of inhibiting both coagulation and complement activation. This significantly highlights the novelty of our work. In addition, while most microfluidic assay is low throughput, the microvessel-on-a-chip platform allows the testing of multiple samples to a scale that allows the use of our 3D assay on a clinical scale.

The microvessels-on-chips permitted high-throughput stimulation of the vascular permeability induced by our EDTA plasma cocktail when spiked with VEGF, histamine, and TNFα. This vessel permeability was confirmed with TEER measurements

by using the ECIS system. However, the ECIS is a 2D-cell based system. The microvessels-on-chips allow us to add physiological relevant cues to the vasculature in vitro with several advantages. For example, cell–cell and cell–ECM interaction and perfusion are considerably reduced in 2D cell culture, which in turn significantly limits their ability to mimic the appropriate level of in vivo cellular responses. Moreover, TEER values vary significantly due to biological and environmental factors. On the other hand, the microvessel-on-a-chip, as a 3D culture system, is a closed system with excellent control and standardization of prepared microvessels with stable endothelial cells.[20,32] With the microvessels-on-chips we could breach the gap between in vitro 2D cell culture and in vivo models, enabling us to accurately predict in vivo permeability.[33] Furthermore, in our high-throughput platform we are dealing with low volume samples. This gives the possibility to do multiple experiments in a cost-effective manner and to reduce blood sampling in patients.

Our microvessel-on-a-chip in combination with our developed plasma screening assay models an aspect of vascular dysfunction seen in COVID-19 patients. This positions us to link disturbed balances in bioactive lipids, cytokines, and other metabolites as seen in COVID-19 patients to their vascular function and helping to understand the pathophysiology of COVID-19. Several mechanisms have been proposed to underlie the systemic vascular endothelium inflammation in severe COVID-19 patients.[34]

First, an excessive cytokine response triggers the expression of proinflammatory cytokines such as type 1 interferons and IL-1, IL-6, and TNFα.[35] This then leads to a systemic proinflammatory activation of endothelial cells.

A second proposed mechanism involves the activation of the bradykinin receptor type 1 (B1). Binding and internalization of angiotensin-converting enzyme 2 by the viral spike proteins[36] can result in an uncontrolled generation of bradykinin, leading to B1-dependent vascular leakage and the pulmonary angioedema that precedes COVID-19 related ARDS.[37] This mechanism may be particularly relevant since the endothelial B1 receptor is markedly upregulated by inflammatory cytokines.[38]

A third mechanism is the excessive intravascular activation of the coagulation system. COVID-19 patients often show clotting disorders, with organ dysfunction and coagulopathy, resulting in higher mortality.[39] These phenomena are known to include occlusion and microthrombosis in small pulmonary vessels in critical COVID-19 patients.[40]

A fourth mechanism, which we propose, is that oxylipins might play a key role in hyperinflammation and hypercoagulation, since there is a significant increase in the secretion of PGF2α in microvessels perfused with COVID-19 plasma samples. PGF2α is an oxylipin enzymatically generated by the oxidation of polyunsaturated fatty acids. During inflammation, reactive oxygen species causes further release of arachidonic acid and cyclooxygenase (COX-2). This contributes to increased production of PGF2α, having a proinflammatory effect in the endothelium.[41,42] Further research should be undertaken in order to investigate the role of oxylipins in COVID-19.

4. Conclusion

This study presents a method to perfuse human blood plasma in the microvessels-on-chips and assess the impact of circulating plasma factors on microvascular integrity. The microvessels-on-chips with human plasma faithfully recapitulated the (patho)physiology of microvessels in vivo that can aid as a sensing platform in clinical trials. The assay enables diagnostic screening of inflammatory or endothelial disrupting plasma factors associated with endothelial dysfunction.

5. Experimental Section

Chip Design: A novel chip configuration (T-design) based on the MIMETAS OrganoPlate platform was designed.

This new design involves a T-junction shown in Figure 1 and Figure S1 (Supporting Information) in which the channels are separated by a phaseguide. The design, due to its geometry, enables easy generation of leak tight vessels and quantification of vascular leakage. Fabrication of the microfluidic devices was carried out by MIMETAS using a previously established protocol.[43] For the experiments with COVID-19 plasma samples, an already established 2-lane OrganoPlate was used by MIMETAS to generate the microvessels.[20]

Cell Culture: HUVECs were isolated from umbilical cord of newborns, collected with informed consent, by an adaption of the method developed by Jaffe et al. in 1973.[44]

The umbilical cord was severed from the placenta soon after birth and placed in a sterile container filled with phosphate-buffered saline (PBS; Fresenius Kabi, The Netherlands) and held at 4 °C until processing. The cord was inspected and at both ends a piece of 1 cm was cut off to remove damaged tissue from clamping. Subsequently, the umbilical vein was cannulated and perfused with PBS to wash out the blood and allowed to drain. When clear fluid flow was observed, the vein was filled with trypsin/EDTA solution (CC-5012, Lonza, USA), placed in the container filled with PBS, and incubated at 37 °C for 20 min. After incubation, the trypsin–EDTA solution containing the endothelial cells was flushed from the cord with air and afterward PBS. The effluent was collected in a sterile 50 mL tube containing 20 mL endothelial cell growth medium 2 (EGM2; C-39216, PromoCell, Germany) supplemented with antibiotics and the cell suspension was centrifuged at 1200 rpm for 7 min. The cell pellet was resuspended in 10 mL EGM2 and cultured on 1% gelatin-coated T75 flasks. Cells were maintained in a 37 °C incubator with 5% CO_2 and the medium was refreshed every other day. After 80% confluency, cells were spilt at 1:3 ratio and cultured in new 1% gelatin-coated T75 flasks at passage 2. Pooled HUVECs (C2519A, Lonza, USA) of 3–6 donors were used for experiments carried out with the COVID-19 plasma samples.

The T-design and 2-lane OrganoPlates were used for all microfluidic cell culture. Thus, the microvascular and ECM channels were separated by phaseguides. Before seeding the cells, 4 mg mL^{-1} rat tail collagen type 1 (3440-005-01, Trevigen) neutralized with 10% 37 g L^{-1} Na_2CO_3 (S5761, Sigma) and 10% 1 M HEPES buffer (15630-056, Gibco) was added in the ECM channels. Subsequently, the collagen was polymerized by incubating the device for 10 min in the incubator at 37 °C and 5% CO_2. The observation windows were filled with 50 µL Hank's Balanced Salt Solution with calcium and magnesium (HBSS+; 24020117, Life Technologies) for optical clarity. The ECM inlets were filled with 20 µL HBSS+ to prevent gel dehydration. The microvascular channels were coated with 1% gelatin for 30 min in the incubator at 37 °C and 5% CO_2. Next, 2 µL of cells were seeded with a density of 20×10^6 cells mL^{-1} in gelatin-coated microvascular channels of the T-design OrganoPlate. Also, 2 µL of cells was seeded with a density of 15×10^6 cells mL^{-1} in gelatin-coated microvascular channels of the 2-lane OrganoPlate. Afterward, the cells were incubated at 37 °C and 5% CO_2 for 1 h to allow cells to adhere. After incubation, 50 µL of EGM2 was added to the inlets and outlets of the microvascular channels of the T-design and 2-lane OrganoPlate. The devices were placed on a rocker platform with a 7° angle of motion and an 8 min timed operation to allow continuous flow of medium in the microvessels. After 24 h, the medium was refreshed and the HUVECs were cultured for an additional 3–4 days to form confluent microvessels.

Coagulation Tests: The prothrombin time (PT) assays and the aPTT assays were performed in the STart Line: STart Max (Diagnostica Stago) and 25×10^{-6} M compstatin (supplied by John Lambris Lab) was used in both assays. EDTA plasma was diluted to 50% plasma with EGM2. For the PT assay, 10×10^{-6} M hirudin (94581-1EA, Sigma-Aldrich) was serial diluted in 50% plasma, 50 µL of each plasma dilution was incubated at 37 °C for 1 min. Coagulation was initiated with 50 µL of Neoplastine Ci Plus 10 (Diagnostica Stago), 1:10 diluted with dilution medium at 37 °C and clotting time was measured. For the aPTT assay, CTI 500 µg mL^{-1} (CTI-01, Haematologic Technologies, Inc.) was serial diluted in 50% plasma and 50 µL of each plasma dilution was incubated at 37 °C for 3 min with 50 µL of aPTT reagent (TriniClot). Coagulation was initiated with 50 µL of 25×10^{-3} M $CaCl_2$ at 37 °C.

Complement Assay: The classical pathway complement activation was measured by activity ELISA.[45] Wells were coated with 2 µg mL^{-1} human IgM in coating buffer (0.1 M $NaHCO_3$, 0.1 M Na_2CO_3, pH 9.6). Plasma samples were diluted in GVB++ (Gelatin Veronal Buffer, with 1×10^{-3} M $MgCl_2$, 2×10^{-3} M $CaCl_2$, 0.05% Tween). The in house made monoclonal antibody RFK22, labeled with digoxigenin (DIG) in incubation buffer (PBS, 0.05% Tween, 1% BSA) was used as a detecting antibody. C3 was measured by using anti-DIG-horseradish peroxidase antibody in incubation buffer (PBS, 0.05% Tween, 1% BSA). Subsequently, the samples were developed with 3,3′,5,5′-Tetramethylbenzidine substrate solution. After 15 min, the reaction was stopped with H_2SO_4 and the optical density was measured at 450 nm.

Plasma Assay: EDTA plasma samples were treated with 1×10^{-6} M hirudin (94581-1EA, Sigma-Aldrich), 50 µg mL^{-1} CTI (CTI-01, Haematologic Technologies), 25×10^{-3} M compstatin and finally recalcified with 3.1×10^{-3} M $CaCl_2$. These treated plasma samples were diluted with basal media (1:1). Finally, this cocktail mix was perfused in the microvessels-on-chips for up to 18 h.

Patient Plasma Samples: The Ethics Review Board of Erasmus MC (MEC-2020-0360) approved the study and participants provided informed consent. The study conformed to the principles outlined in the Declaration of Helsinki. The pooled EDTA plasma samples were from male and female COVID-19 intensive care patients at the age of 59 and above. These patients were on medication and were divided into the early and late stages of disease progression.

COVID-19 patients (n = 8) with early stage disease and having a marked thrombotic disorder were ES. COVID-19 patients (n = 8) who are in proinflammatory stage (cytokine storm) were LS. The IL-6 concentrations of the COVID-19 patients were 200–1200 pg mL^{-1}. Left over EDTA plasma samples of subjects without history of cardiovascular-related diseases were used as control.

Vascular Leakage Assay: Endothelial cell culture media and plasma samples of healthy controls were spiked with vascular endothelial growth factor (VEGF; 450-32, PeproTech), histamine (H7125 SIGMA, Sigma-Aldrich) or tumor necrosis factor alpha (TNFα; H8916 SIGMA, Sigma-Aldrich). To measure vessel permeability, the ECM channel inlets were refreshed with 20 µL HBSS+. Then, the media in the inlets and outlets of the microvascular channels were replaced with 40 and 30 µL of 125 µg mL Albumin-Alexa 555 (A34786, Life Technologies). Following this, the OrganoPlate was placed in the environmental chamber (37 °C; 5% CO_2) of a high-content confocal microscope (Molecular Devices, ImageXpress Micro Confocal) and time-lapse images were captured. The permeability is measured by acquiring images in one min intervals. As high-content microscope is able to image all 96 devices within a minute, the total measurement takes 10 min.

The permeability coefficient was calculated by determining the fluorescent intensities in the microvascular channel of captured images. At the same time, the fluorescent intensities in the ECM channel of the capture images was obtained and normalized with the fluorescent intensities in the microvascular channel of each measured time point. This showed the change in intensity ratio inside the gel channel as a function of time. The scatter plot was fitted with a linear trend line to determine the slope. Finally, using Fick's first law the apparent permeability was determined as[20,46]

$$P_{app}\left(\cdot 10^{-6}\ cm\,s^{-6}\right) = \frac{d\left(\frac{I_g}{I_p}\right)}{dt} \cdot \frac{A_g}{I_w} \quad (1)$$

where I_p is the intensity in the microvascular channel, I_g is the intensity in the ECM channel, A_g (480×10^{-6} cm^2 in T-design and 96×10^{-4} cm^2 in 2-lane) is the area of the ECM channel, and l_w (400×10^{-4} cm in T-design and 0.436 cm in 2-lane) is the length of the vessel wall that separates between ECM and microvascular region. All data analysis was done with ImageJ and Matlab (2016a, MathWorks).

Transendothelial Electrical Resistance Measurements: Cell barrier function was assessed by measuring TEER in real time using the electric cell–substrate impedance sensing (ECIS Zθ, Applied BioPhysics) system. HUVECs at a density of 15×10^3 cells per well were dispensed and grown to a confluent monolayer on 1% gelatin-coated 96W20idf electrodes (Applied BioPhysics) in 200 µL EGM2 in a 5% CO_2 incubator at 37 °C for 48 h. For the coating, gelatin was dissolved in water. Monolayer resistance was recorded at 4 kHz over 15 min intervals for baseline measurement. Subsequently, 75 µL medium was taken out and 75 µL recalcified 50% EDTA-plasma with 1×10^{-6} M hirudin, 50 µg mL^{-1} CTI and 25×10^{-6} M compstatin was added for 6 h before treatment. After 6 h, 75 µL of the EDTA plasma cocktail and medium were replaced by 75 µL of the plasma cocktail and medium spiked with VEGF, histamine, and TNFα.

For analysis of changes in barrier function, TEER measurements were averaged over the last ten stable pretreatment time points as baseline. For the percentage resistance, TEER values were corrected for the base line.

Immunocytochemistry: The medium was aspirated from the medium inlets and outlets of the chips and cells were fixed using 4% paraformaldehyde in HBSS+ for 10 min at room temperature. The fixative was aspirated and cells were rinsed once with HBSS+. Next, cells were permeabilized for two min with 0.2% Triton X-100 in HBSS+ and washed once with HBSS+. The cells were blocked with 5% BSA in HBSS+ for 30 min and incubated with primary antibody solution overnight at 4 °C. Mouse anti-human VE-cadherin (CD144, 1:100; 555661, BD Biosciences) was used as the primary antibody. The wells were washed with HBSS+, followed by the addition of Hoechst (1:2000; H3569, Invitrogen), rhodamine phalloidin (1:200; P1951 SIGMA, Sigma-Aldrich) and secondary antibody solution containing goat-anti-mouse Alexa Fluor 488 (1:250; R37120, Waltham). After 1 h of incubation in the dark at room temperature, wells were washed three times with HBSS+. High quality Z-stack images of the stained cells were obtained using a high-content confocal microscope (ImageXpress Micro Confocal, Molecular Devices). The images were processed with ImageJ.

Metabolic Profiling: Plasma samples of four microvessels were pooled to form one sample to allow analyses of metabolites at low concentrations due to low cell numbers. For metabolite extraction, sample preparation procedure was performed according to the in-house validated protocol which has been optimized on previously published method[47] and successfully applied for signaling lipid profiling.[48] Briefly, plasma samples (150 μL) were added with 5 µL antioxidant solution and 10 µL internal standards. Acidified with citric acid/phosphate buffer (pH 4.5), all samples were then dealt with liquid–liquid extraction with 1 mL of butanol and methyl tert-butyl ether (1:1 v/v). Samples were vortexed, centrifuged, and then the organic phase was collected and dried. After reconstitution with ice-cold 70% methanol/30% acetonitrile injection solution, each sample was again vortexed and centrifuged and the supernatant was transferred to the insert in a glass vial. UPLC-MS/MS based analysis was then applied for low-pH measurement (Sciex Qtrap 6500+ coupled with Shimadzu LC-30AD). Sciex OS was applied to accomplish all the peak determination and integration. For the metabolite PGF2α, the response ratio was obtained by calculating the ratio of peak area of the target compound to the peak area of the assigned internal standard.

Statistical Analysis: For statistical analyses, IBM SPSS Statistics 23 was used. Values are given as mean ± standard error of the mean (SEM). Multiple comparisons were made by one-way ANOVA followed

by Dunnett's test or Tukey's multiple comparison test. Results were considered significant at $*P < 0.05$, $**P < 0.01$, $***P < 0.001$.

Supporting Information

Supporting Information is available from the Wiley Online Library or from the author.

Acknowledgements

The authors like to thank John Lambris for providing compstatin in this study. This study was financially supported by the Dutch Heart Foundation CVON RECONNECT consortium and a ZonMW MKMD grant (114022501). Additional support was obtained from NWO-TTW (IMMUNMET, Grant No. 16249), TKI METABOCHIP project, ZonMW Health Holland HHOOCS grant Stabilise, Dutch Heart Foundation (Grant Nos. 2013T127 and 2018T095), and the LSH PPS grant METACOVID.

Conflict of Interest

TH is cofounder and shareholder of MIMETAS. All other authors declare no conflict of interest related to the content of this manuscript.

Data Availability Statement

The data that supports the findings of this study are available in the supplementary material of this article.

Keywords

blood, endothelial cells, in vitro models, microfluidics, organs-on-chips, permeability, vasculature

Received: May 17, 2021
Revised: September 7, 2021
Published online: September 29, 2021

[1] D. Mozaffarian, E. J. Benjamin, A. S. Go, D. K. Arnett, M. J. Blaha, M. Cushman, S. R. Das, S. de Ferranti, J. P. Despres, H. J. Fullerton, V. J. Howard, M. D. Huffman, C. R. Isasi, M. C. Jimenez, S. E. Judd, B. M. Kissela, J. H. Lichtman, L. D. Lisabeth, S. M. Liu, R. H. Mackey, D. J. Magid, D. K. McGuire, E. R. Mohler, C. S. Moy, P. Muntner, M. E. Mussolino, K. Nasir, R. W. Neumar, G. Nichol, L. Palaniappan, D. K. Pandey, M. J. Reeves, C. J. Rodriguez, W. Rosamond, P. D. Sorlie, J. Stein, A. Towfighi, T. N. Turan, S. S. Virani, D. Woo, R. W. Yeh, M. B. Turner, A. H. A. S. C. Stroke, *Circulation* **2016**, *133*, 447.
[2] M. Finsterbusch, M. B. Voisin, M. Beyrau, T. J. Williams, S. Nourshargh, *J. Exp. Med.* **2014**, *211*, 1307.
[3] K. Gupta, P. Gupta, R. Wild, S. Ramakrishnan, R. P. Hebbel, *Angiogenesis* **1999**, *3*, 147.
[4] M. L. Valle, J. Dworshak, A. Sharma, A. S. Ibrahim, M. Al-Shabrawey, S. Sharma, *Exp. Eye Res.* **2019**, *178*, 27.
[5] A. Junaid, J. Schoeman, W. Yang, W. Stam, A. Mashaghi, A. J. van Zonneveld, T. Hankemeier, *eLife* **2020**, *9*, 54754.
[6] A. Junaid, H. Q. Tang, A. van Reeuwijk, Y. Abouleila, P. Wuelfroth, V. van Duinen, W. Stam, A. J. van Zonneveld, T. Hankemeier, A. Mashaghi, *iScience* **2020**, *23*, 100765.
[7] T. P. Schmidt, C. Goetz, M. Huemer, G. Schneider, S. Wessler, *Gut Pathog.* **2016**, *8*, 29.
[8] C. M. Niessen, D. Leckband, A. S. Yap, *Physiol. Rev.* **2011**, *91*, 691.
[9] N. R. Wevers, R. van Vught, K. J. Wilschut, A. Nicolas, C. W. Chiang, H. L. Lanz, S. J. Trietsch, J. Joore, P. Vulto, *Sci. Rep.* **2016**, *6*, 38856.
[10] E. Ulker, W. H. Parker, A. Raj, Z. C. Qu, J. M. May, *Mol. Cell. Biochem.* **2016**, *412*, 73.
[11] C. Park-Windhol, P. A. D'Amore, *Annu. Rev. Pathol.:Mech. Dis.* **2016**, *11*, 251.
[12] K. Ashina, Y. Tsubosaka, T. Nakamura, K. Omori, K. Kobayashi, M. Hori, H. Ozaki, T. Murata, *PLoS One* **2015**, *10*, 0132367.
[13] T. J. Rabelink, H. C. de Boer, A. J. van Zonneveld, *Nat. Rev. Nephrol.* **2010**, *6*, 404.
[14] I. K. Zervantonakis, S. K. Hughes-Alford, J. L. Charest, J. S. Condeelis, F. B. Gertler, R. D. Kamm, *Proc. Natl. Acad. Sci. USA* **2012**, *109*, 13515.
[15] H. Kidoya, H. Naito, N. Takakura, *Blood* **2010**, *115*, 3166.
[16] A. Schaefer, T. J. van Duijn, J. Majolee, K. Burridge, P. L. Hordijk, *J. Immunol.* **2017**, *198*, 4823.
[17] M. A. Lindorfer, E. M. Cook, E. S. Reis, D. Ricklin, A. M. Risitano, J. D. Lambris, R. P. Taylor, *Clin. Immunol.* **2016**, *171*, 32.
[18] Y. Z. Zhang, D. W. Shao, D. Ricklin, B. M. Hilkin, C. M. Nester, J. D. Lambris, R. J. H. Smith, *Immunobiology* **2015**, *220*, 993.
[19] R. Zhang, X. B. Wang, L. Ni, X. Di, B. T. Ma, S. Niu, C. W. Liu, R. J. Reiter, *Life Sci.* **2020**, *250*, 117583.
[20] V. van Duinen, A. van den Heuvel, S. J. Trietsch, H. L. Lanz, J. M. van Gils, A. J. van Zonneveld, P. Vulto, T. Hankemeier, *Sci. Rep.* **2017**, *7*, 18071.
[21] W. B. Mitchell, *Paediatr. Respir. Rev.* **2020**, *35*, 20.
[22] B. D. Hammock, W. Wang, M. M. Gilligan, D. Panigrahy, *Am J Pathol* **2020**, *190*, 1782.
[23] K. Kobayashi, D. Horikami, K. Omori, T. Nakamura, A. Yamazaki, S. Maeda, T. Murata, *Sci. Rep.* **2016**, *6*, 32109.
[24] S. Jiang, R. Xia, Y. Jiang, L. Wang, F. Gao, *PLoS One* **2014**, *9*, 86407.
[25] E. Lundeberg, A. M. Van Der Does, E. Kenne, O. Soehnlein, L. Lindbotn, *Arterioscler., Thromb., Vasc. Biol.* **2015**, *35*, 783.
[26] D. T. T. Phan, X. L. Wang, B. M. Craver, A. Sobrino, D. Zhao, J. C. Chen, L. Y. N. Lee, S. C. George, A. P. Lee, C. C. W. Hughes, *Lab Chip* **2017**, *17*, 511.
[27] H. Ryu, S. Oh, H. J. Lee, J. Y. Lee, H. K. Lee, N. L. Jeon, *JALA* **2015**, *20*, 296.
[28] B. M. Maoz, A. Herland, E. A. FitzGerald, T. Grevesse, C. Vidoudez, A. R. Pacheco, S. P. Sheehy, T. E. Park, S. Dauth, R. Mannix, N. Budnik, K. Shores, A. Cho, J. C. Nawroth, D. Segre, B. Budnik, D. E. Ingber, K. K. Parker, *Nat. Biotechnol.* **2018**, *36*, 865.
[29] B. Nilsson, R. Larsson, J. Hong, G. Elgue, K. N. Ekdahl, A. Sahu, J. D. Lambris, *Blood* **1998**, *92*, 1661.
[30] A. Jain, R. Barrile, A. D. van der Meer, A. Mammoto, T. Mammoto, K. De Ceunynck, O. Aisiku, M. A. Otieno, C. S. Louden, G. A. Hamilton, R. Flaumenhaft, D. E. Ingber, *Clin. Pharmacol. Ther.* **2018**, *103*, 332.
[31] R. Barrile, A. D. van der Meer, H. Park, J. P. Fraser, D. Simic, F. Teng, D. Conegliano, J. Nguyen, A. Jain, M. Zhou, K. Karalis, D. E. Ingber, G. A. Hamilton, M. A. Otieno, *Clin. Pharmacol. Ther.* **2018**, *104*, 1240.
[32] R. Ghaffarian, S. Muro, *J. Vis. Exp.* **2013**, *80*, 50638.
[33] J. Lee, G. D. Lilly, R. C. Doty, P. Podsiadlo, N. A. Kotov, *Small* **2009**, *5*, 1213.
[34] C. Magro, J. J. Mulvey, D. Berlin, G. Nuovo, S. Salvatore, J. Harp, A. Baxter-Stoltzfus, J. Laurence, *Transl. Res.* **2020**, *220*, 1.
[35] E. Prompetchara, C. Kettoy, T. Palaga, *Asian Pac. J. Allergy Immunol.* **2020**, *38*, 1.

[36] A. C. Walls, Y. J. Park, M. A. Tortorici, A. Wall, A. T. McGuire, D. Veesler, *Cell* **2020**, *181*, 281.
[37] Y. Imai, K. Kuba, S. Rao, Y. Huan, F. Guo, B. Guan, P. Yang, R. Sarao, T. Wada, H. Leong-Poi, M. A. Crackower, A. Fukamizu, C. C. Hui, L. Hein, S. Uhlig, A. S. Slutsky, C. Y. Jiang, J. M. Penninger, *Nature* **2005**, *436*, 112.
[38] G. F. Passos, E. S. Fernandes, M. M. Campos, J. G. V. C. Araujo, J. L. Pesquero, G. E. P. Souza, M. C. W. Avellar, M. M. Teixeira, J. B. Calixto, *J. Immunol.* **2004**, *172*, 1839.
[39] N. Tang, D. J. Li, X. Wang, Z. Y. Sun, *J. Thromb. Haemostasis* **2020**, *18*, 844.
[40] M. Oudkerk, H. R. Buller, D. Kuijpers, N. van Es, S. F. Oudkerk, T. McLoud, D. Gommers, J. van Dissel, H. Ten Cate, E. J. R. van Beek, *Radiology* **2020**, *297*, E216.
[41] M. S. K. Wong, P. M. Vanhoutte, *Acta Pharmacol. Sin.* **2010**, *31*, 1095.
[42] R. Dworski, L. J. Roberts, J. J. Murray, J. D. Morrow, T. V. Hartert, J. R. Sheller, *Clin. Exp. Allergy* **2001**, *31*, 387.
[43] P. Vulto, S. Podszun, P. Meyer, C. Hermann, A. Manz, G. A. Urban, *Lab Chip* **2011**, *11*, 1596.
[44] E. A. Jaffe, R. L. Nachman, C. G. Becker, C. R. Minick, *J. Clin. Invest.* **1973**, *52*, 2745.
[45] M. A. Seelen, A. Roos, J. Wieslander, T. E. Mollnes, A. G. Sjoholm, R. Wurzner, M. Loos, F. Tedesco, R. B. Sim, P. Garred, E. Alexopoulos, M. W. Turner, M. R. Daha, *J. Immunol. Methods* **2005**, *296*, 187.
[46] V. H. Huxley, F. E. Curry, R. H. Adamson, *Am. J. Physiol.* **1987**, *252*, H188.
[47] J. C. Schoeman, A. C. Harms, M. van Weeghel, R. Berger, R. J. Vreeken, T. Hankemeier, *Anal. Bioanal. Chem.* **2018**, *410*, 2551.
[48] A. Di Zazzo, W. Yang, M. Coassin, A. Micera, M. Antonini, F. Piccinni, M. De Piano, I. Kohler, A. C. Harms, T. Hankemeier, S. Boinini, A. Mashaghi, *J. Mol. Med.* **2020**, *98*, 751.